Astron. Astrophys. 331, 251–261 (1998)

ASTRONOMY AND ASTROPHYSICS

Broad band X-ray spectrum of Cygnus X-1

V.R. Chitnis, A.R. Rao, and P.C. Agrawal

Tata Institute of Fundamental Research, Homi Bhabha Road, Mumbai(Bombay) 400 005, India

Received 22 April 1997 / Accepted 20 October 1997

Abstract. We present the hard X-ray (20 − 100 keV) observations of Cygnus X-1 obtained using a large area balloon-borne Xenon filled Multi-anode Proportional Counter (XMPC) telescope. The observations were carried out during the γ_2 state of the source and we obtain a power law photon index of 1.62±0.07. To constrain the spectral shape of the source, we have analyzed the archival EXOSAT ME argon and GSPC data in the low energies (2 − 20 keV band) as well as the archival OSSE data in the high energies (50 − 500 keV). The data in different energy bands are not obtained in simultaneous observations, but they pertain to the γ_2 state of the source. We have attempted a combined fit to the wide band data using appropriate mutual detector calibrations. This method implicitly assumes that the variations in the source intensity in the γ_2 state is mainly due to the variations in the normalisations of the spectral components rather than any change in the spectral parameters. A combined fit to the EXOSAT and XMPC data (2 − 100 keV) shows that the observed spectrum requires a low energy absorption corresponding to the Galactic interstellar absorption, a low energy excess modeled as a blackbody, a narrow emission line due to iron K_α and a continuum. The continuum can be either modeled as a power law with a reflection bump or a Comptonisation model with an additional bump which can be modeled as the partial covering with a heavy absorber. To resolve between these two models, we have attempted a combined fit to the 2 − 500 keV data obtained from EXOSAT, XMPC and OSSE. We find that a single Comptonisation model cannot adequately represent the continuum. The observed excess is at higher energies (about 100 keV) and it cannot be modeled as reflection of power law or Comptonisation model. We find that a two component Comptonisation model adequately represents the data. We explore the possible emission region that is responsible for the observed spectrum.

Key words: X-rays: stars – stars: individual: Cyg X-1

1. Introduction

Cygnus X-1 is a well-known Galactic black hole candidate studied extensively by almost every X-ray astronomy experiment since its discovery. It shows two distinct spectral states, 'low' and 'high', depending on its soft X-ray flux. Soft X-ray spectrum changes drastically between these two states (with an equivalent power law photon index changing from ∼1.5 to > 3-4), whereas hard X-ray (20 − 100 keV) spectrum is described by a power law with photon index ranging from 1.2 to 2.3 at all times (Liang and Nolan 1984). Low state soft X-ray continuum (2 − 10 keV) of Cyg X-1 is generally characterized as a power law with a photon index of about 1.5. Barr and van der Woerd (1990) detected the presence of a soft excess in a combined fit to the EXOSAT Transmission Grating Spectrometer (TGS) data (0.4 − 2 keV) and Gas Scintillation Proportional Counter (GSPC) data (2 − 12 keV), which they have modeled as a steep power law and a broad emission feature between 550 eV and 800 eV. Similar results were obtained by Balucinska and Hasinger (1991) while analyzing the EXOSAT Medium Energy (ME) data (1.3 − 15 keV). They modeled the soft excess as a blackbody with kT ∼ 0.3 keV. The BBXRT observations probably did not detect this component (Marshall et al. 1993). Analyzing the Rosat PSPC data over 0.1 − 2 keV near the binary orbital phase of 0.5, Balucinska-Church et al. (1995) characterized the soft excess with a blackbody with temperature kT = 0.13±0.02 keV.

Barr et al. (1985) discovered iron K_α line in Cyg X-1 using the EXOSAT GSPC data. They found it to be red-shifted (center at 6.2 keV), broad (∼ 1.2 keV) and weak (equivalent width ∼ 120 eV). Kitamoto et al. (1990) detected the iron line centered at 6.5 keV using the Tenma GSPC data. Kitamoto et al. (1984) also detected an absorption edge at 7.18±0.18 keV only during a dip, whereas Balucinska-Church and Barr (1991) saw an edge at 7.1 − 7.8 keV during persistent emission implying ionisation state between neutral to FeXVII. Tanaka (1991) and Ebisawa (1991) modeled the Cyg X-1 spectrum (from Ginga observations) using reflection of power-law and Gaussian line and found iron line and edge at 6.4 keV and 7.2 keV respectively, corresponding to neutral iron. They also showed that the line is red-shifted (6.1 keV) if the continuum is fitted by power-law only. Done et al. (1992) analyzed EXOSAT ME Ar, GSPC and HEAO1-A2 data and fitted it with a Compton reflection of power-law photons with photon index ∼ 1.8, from an ionized disk. The observed average iron line energy is 6.44±0.12 keV and the line is found to be narrow. BBXRT spectrum over 3 − 11.2 keV is consistent with a disk reflection without indication of ionisation, and with

Send offprint requests to: A.R. Rao, (arrao@tifrvax.tifr.res.in)

little evidence of line emission, with a possible exception of a narrow emission line at 6.4 keV with an equivalent width of 13±11 eV (Marshall et al. 1993). Ebisawa et al. (1996) detected an iron line at 6.4 keV with intrinsic width of $\leq$ 0.2 keV and equivalent width of 10 − 30 eV along with a broad edge feature in the ASCA SIS data.

The hard X-ray spectrum of Cyg X-1 over the energy range of 20 − 200 keV (Sunyaev and Trumper 1979) was fitted by a thermal Compton model (Sunyaev and Titarchuk 1980; hereafter referred to as the CompST model) with an electron temperature of kT_e = 27 keV and optical depth τ = 5, in order to account for the steepening of the spectrum above 100 keV. While fitting broad band data over the energy range of 3 keV to 8 MeV, obtained from HEAO − 1, Nolan et al. (1981) found that a single CompST model is insufficient to fit the data and they used two Comptonisation models with temperatures kT_e of 15.2 and 41.6 keV, respectively.

The presence of a 'super-low' state in Cyg X-1, characterized by a decrease in both the soft and hard X-ray flux, was first detected by Ling et al. (1983) while analyzing data from JPL high resolution gamma ray spectrometer on board HEAO-3. Fitting the data over 48 − 300 keV range they concluded that the hard X-ray spectrum does not change much between the 'super-low' and the 'low' state, whereas it is quite different during the 'high' state. In an extension of this work, Ling et al. (1987) divided the hard X-ray (45 − 140 keV) states of Cyg X-1 into a γ_1 state (corresponding to the 'super-low' state), a γ_2 state (the 'normal' state to which the source frequently returns) and the infrequently occurring γ_3 ('flare') state. Salotti et al. (1992) fitted the 35 − 750 keV data obtained from the SIGMA detectors on board GRANAT satellite using CompST model with kT_e = 62 keV and τ = 2. Grebenev et al. (1993) extended this fit to lower energies in attempting a combined fit for ART-P (2 − 60 keV) and SIGMA data and found that it overestimated flux at lower energies, whereas simultaneous fit over the energy range 2 − 600 keV with CompST (kT_e = 37 keV and τ = 1.5) underestimated the flux at higher energies ($>$ 100 keV).

Döbereiner et al. (1995) fitted HEXE spectrum over 2 − 200 keV range pertaining to the γ_2 state of the source with Compton reflection of power-law (α = 1.64±0.01) from cool matter with covering factor of 0.59±0.04. This model provided better fit than a power-law or CompST model to the HEXE data. Phlips et al. (1996) fitted Cyg X-1 spectral data over 50 keV − 1 MeV obtained from OSSE on board CGRO with various models and found that the exponentially truncated power-law with a photon index 1.39±0.02 and cutoff energy kT = 158±3 keV give a fit to the data better than thermal bremsstrahlung or thermal Comptonisation model. COMPTEL data over the energy range 0.75 − 30 MeV obtained in June and August 1991 are described by Wien spectral model (high energy limit of CompST) with plasma temperatures 192±27 keV and 204±21 keV, respectively (McConnell et al. 1994).

Most of the attempts so far to explain the energy spectrum of Cyg X-1 were over limited dynamic range and even when data over wider band-widths were used, they were generally from detectors of poor energy resolution. To understand the nature of the underlying continuum it is necessary to have good energy resolution at lower energies, wider band-width at higher energies to include the turnover at $>$ 200 keV, and medium energy resolution at the intermediate (20 − 100 keV) energies. We have achieved this by combining data obtained by us in a balloon flight of Xenon filled Multi-anode Proportional Counters (XMPCs) over energy range of 20 − 100 keV, with EXOSAT ME Argon and GSPC data in 2 − 20 keV band and OSSE data over 50 − 500 keV range. We have carried out a simultaneous fit to these data sets pertaining to the γ_2 state of the source. Since the source generally remains in this state with a flux variation of less than a factor of 2, we have derived the spectral parameters under the assumption that the flux variation pertains to only the normalisation constants of the various spectral components rather than the spectral parameters.

The paper is organized as follows. In Sect. 2 we describe of the XMPC observations, details of the response matrix of the detectors and the results obtained from a spectral fit to the Cyg X-1 data. In Sect. 3 we describe a wide band spectral model for Cyg X-1. The results are discussed in Sect. 4 followed by summary in the last section.

2. XMPC instrument details and observations

Hard X-ray observations of Cyg X-1 were carried out in a balloon flight of a telescope consisting of two xenon filled multi-anode proportional counters (XMPCs) each with an area of 1230 cm^2, carried out on 1992 April 5/6 from Hyderabad, India. These detectors have an average X-ray detection efficiency of about 50% between 20 and 100 keV. Active volume of the detectors is divided into three layers, with four anode cells of cross-sectional area 4.8 cm × 4.8 cm in each layer. Alternate anode cells in each layer are joined together. The anode cell assembly is surrounded by veto cells on three sides. In order to reduce background induced by charged particles, anode cells are operated in mutual anti-coincidence to reject simultaneous events from different anodes. To avoid rejection of genuine X-ray events above 34.5 keV, escape gating technique is used, which accepts two simultaneous events, provided one of them is in 25 to 35 keV band, corresponding to the xenon K-shell fluorescent event. In case of the escape gated event, only non-K event is analyzed for the pulse height and the energy of the K-shell fluorescent event is assumed to be 29.7 keV. The veto layer is operated in anti-coincidence with the main detection cells to reject background induced by charged particles. A mechanical graded slat collimator of tin and copper restricts the field of view to 5° × 5° FWHM. For details of the X-ray telescope refer to Rao et al. (1987, 1991).

The balloon flight was carried out on 1992 April 5 at 19:01 UT, and the balloon reached a ceiling altitude corresponding to a residual atmospheric column density of 4 gm cm^{-2} at 21:15 UT. The payload is oriented using an alt-azimuth orientation system with a pointing accuracy of 0.3°. Source tracking is done according to azimuth and elevation angles stored in an on-board programmer, which are updated every minute. Cyg X-1 was observed continuously for a duration of one hour starting

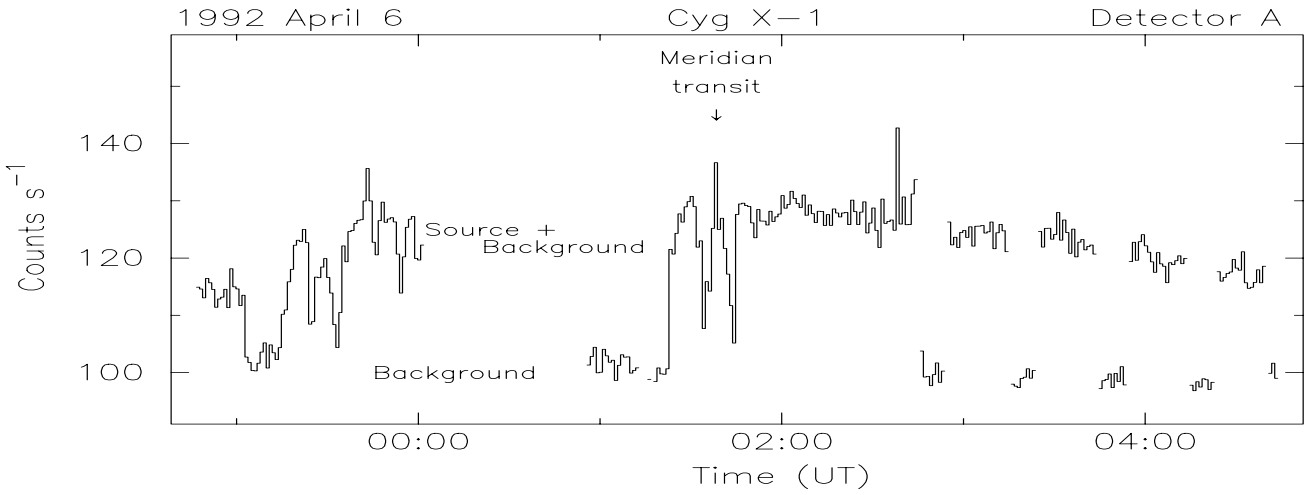

Fig. 1. The count rate profile of Cyg X-1 obtained from a balloon flight carried out on 1992 April 5/6 using the XMPC detector. The source and background observations are marked in the figure. The decrease in the source count rate after the meridian transit is due to increase in the air mass. During the initial part of the observation the source was scanned across for aspect calibration. The increase in the count rate around 02:50 is due to a gamma-ray burst.

at 1:50 UT on 1992 April 6, followed by 4 cycles of source and background observations, for 20 and 10 minutes, respectively. Count rate profile of Cyg X-1 obtained from one of the XMPCs during this balloon flight is shown in Fig. 1. The effect of change in air mass shows as a decrease in the source count rate away from the meridian transit time. As can be seen from the figure, the background count rate remained steady throughout the observations. The gap in the observation before the meridian transit is the duration for which the source NGC 4151 was being tracked. Aspect calibration by the triangulation method is attempted several times during the beginning of the observations. From a detailed fitting of the variation of count rates during aspect calibration and also with the zenith angle of the source, we estimate that the error in the orientation of the telescope can contribute to an extra vignetting correction of about 0.2 (corresponding to an angular offset of 1°). Increase in the count rate for a duration of about 10 minutes at the end of the one hour tracking is due to a gamma-ray burst. Average Cygnus X-1 count rate near the meridian transit was 25.5 ± 0.4 counts s^{-1}, after subtracting the background count rate.

2.1. Detector response matrix

In order to characterize the energy spectra of X-ray sources it is necessary to have a detailed knowledge of the response of the detector. Fig. 2 shows the response of a single anode of a detector for fluorescent K_α and K_β X-rays from Tb. Various photo-peaks and escape peaks can be seen. The energy resolution of the detector is $\sim 9.5\%$ at 44 keV and it shows a weak dependence on energy. As can be seen from the figure, xenon gas has a very large fluorescence yield and to take care of such effects, we have generated response matrix of the XMPC using a Monte Carlo routine. Inputs to this program include detector characteristics such as partial pressure of xenon gas in the detector, layer-wise conversion gain (relation between output pulse height and input energy), energy resolution of the detector, geometry of the detector, and characteristics of event selection logic such as thresholds of K-band, thresholds of upper and lower level discriminators which defines energy range of acceptable events. In the simulation program, each photon is tracked assuming random incidence at the detector surface. Position and layer number for the interaction is then calculated. Possibility of emission of K-X-ray is considered and layer number corresponding to interaction of the K-X-rays is calculated. Taking into account gain and energy resolution of the detector, the output pulse height is evaluated. Escape gating technique is taken into consideration by calculating pulse height only for non-K event in case of simultaneous events. Depending on the type of interaction and the layer in which the interaction took place, a layer identification number is generated. Simulation is done typically 10000 times for each energy bin of width 1 keV, between 10 and 130 keV. The corrections due to absorption in the air and the window material are calculated numerically.

Various inputs to this routine, e.g. layer-wise gain and energy resolution of the detector, various event selection logic thresholds etc., are computed by calibrating the detectors with various radioactive X-ray sources of known energies. The observed response of the detector to mono-energetic X-rays is compared with the simulated one. It was found that one of the detectors had better uniformity of gain and overall energy resolution (10% FWHM at 60 keV) and the observed spectra from calibration sources were found to show good agreement with the predicted spectra correct to about 2% in each spectral bin.

Fig. 3 shows the response of the second layer of the detector A for Am^{241} radioactive source. Data points with error bars correspond to the observed pulse height distribution and the histogram corresponds to the predicted pulse height distribution obtained by convolving a Gaussian line at 60 keV with the Monte

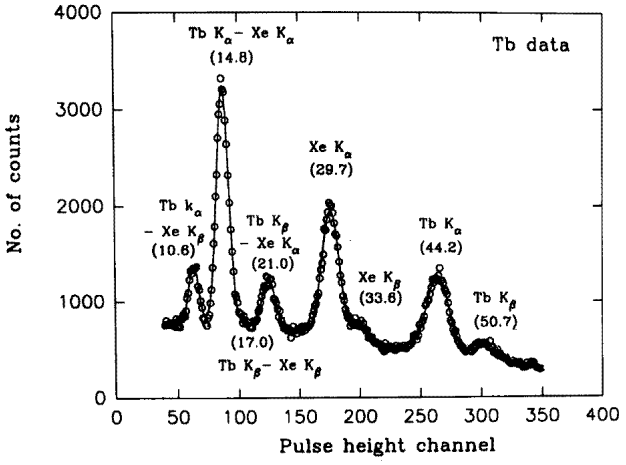

Fig. 2. Response of the detector for characteristic X-rays from Tb radioactive source. Various peaks including photo peaks and escape peaks are marked.

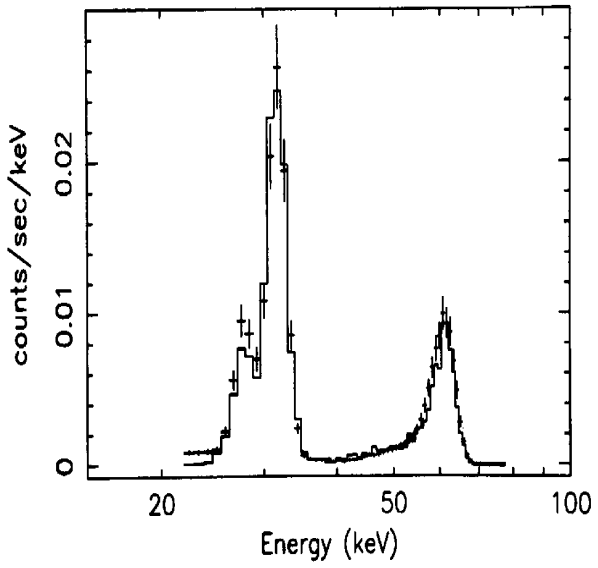

Fig. 3. Response of layer 2 of detector A for Am^{241} source. Data points with error bars correspond to the observed pulse height distribution and histogram corresponds to the predicted pulse height distribution for a Gaussian line at 60 keV, convolved through the Monte Carlo simulated response of the detector.

Carlo simulated response of the detector. Am^{241} photo-peak at 60 keV and two escape peaks at 26 and 29.9 keV corresponding to the escape of xenon K_β and K_α X-rays can be seen in the figure.

2.2. Hard X-ray spectrum of Cyg X-1

We have selected data from the continuous tracking of Cyg X-1 near meridian transit, from one of the detectors which has better spectral response, for spectral fitting. The spectral files are generated for separate layers and data for each layer are re-binned in 42 channels. We have used the XSPEC package

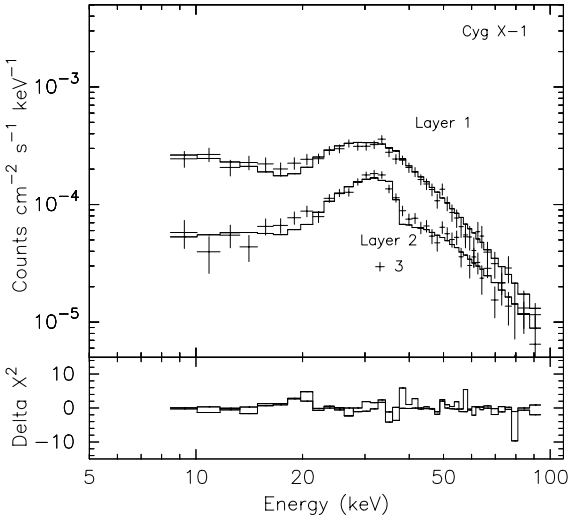

Fig. 4. Observed count rate spectra from Cyg X-1 obtained from XMPC, shown separately for layer 1 and bottom 2 layers. The best fit power-law model with photon index (Γ) of 1.62, convolved through the detector response is shown as histograms. The residuals to the model fit are shown in the lower panel of the figure as contribution to the χ^2.

(Arnaud 1996) for the spectral fitting. Simultaneous spectral fits for the three layers were carried out. A power-law with a photon index (Γ) of 1.62±0.07 (90% confidence limits) gives an acceptable value of χ^2_{min} of 129 for 125 degrees of freedom (dof). The observed $20-100$ keV flux is 1.3×10^{-8} ergs cm^{-2} s^{-1}, which corresponds to a luminosity of 0.9×10^{37} ergs s^{-1} (for a distance of 2.5 kpc). The observed flux density at 100 keV is 6.4×10^{-4} photons cm^{-2} s^{-1} keV^{-1}. The observed count spectra obtained from layer 1 and layer 2 and 3 summed together, are shown in fig. 4. The best fit power-law spectrum, convolved with the detector response is shown as histograms. The residuals to the fit are shown in lower panel, as contribution to χ^2.

We have also made an attempt to fit other spectral models to the XMPC data. Thermal bremsstrahlung model gives a χ^2_{min} of 126 for 125 dof, with temperature >126 keV. The CompST model gives χ^2_{min} of 123 for 124 dof, with electron temperature kT_e of 25^{+18}_{-6} keV and the optical depth τ of $4.8^{+1.6}_{2.4}$ (90% confidence errors for 2 free parameters). Due to limited bandwidth of the data we cannot distinguish between any of these models.

In order to know the exact nature of the continuum, which is not possible due to the limited dynamic range of the XMPC data, we have extended the dynamic range by combining XMPC data with EXOSAT ME Argon and GSPC data spanning $2-20$ keV band and OSSE data over $50-500$ keV. The source normally remains in the γ_2 state, occasionally going to the super-low (γ_1) or the flare (γ_3) state (Ling et al. 1987). The flux density at 100 keV derived from power-law spectral model for XMPC data agrees well with the average value derived from 10 observations from the SIGMA detector (6.37×10^{-4} photons cm^{-2} s^{-1} keV^{-1}) made between 1990 March and 1992 March, when the source

was in γ_2 state (Laurent et al. 1993), and hence we can conclude that the source was in the γ_2 state during our observations. We have selected EXOSAT and OSSE data pertaining to γ_2 state of Cyg X-1 and carried out simultaneous fit to EXOSAT, XMPC and OSSE data spanning an energy range of $2 - 500$ keV.

3. Wide band spectrum of Cyg X-1

3.1. The EXOSAT data and simultaneous spectral fit to EXOSAT and XMPC data

The EXOSAT archive contains spectral data obtained from medium energy (ME) argon filled (Ar) detectors and gas scintillation proportional counters (GSPC). The Ar detectors have an area of ~ 1600 cm^2 and they are sensitive in 1 to 20 keV range (Turner, Smith and Zimmerman 1981). The ME data is available in 128 pulse height (PH) channels (extending to 60 keV) or in 64, 32 or 8 channels (extending to 20 keV). The GSPC, although having a smaller area (≈ 150 cm^2), has an energy resolution that is a factor of 2 better than the Ar detectors (Peacock et al. 1981). The GSPC can operate at gain 2 covering an energy range of $2 - 16$ keV in 256 PH channels or gain 1 covering 4 $- 32$ keV in 256 PH channels (Peacock et al. 1981).

We have used the criteria of Done et al. (1992) for selecting the EXOSAT data, viz., selecting good quality data without absorption dips, with proper background subtraction and good spectral binning. There are 5 GSPC and 4 ME spectra which satisfy the criteria. Further, in order to carry out combined fit for the ME and the GSPC data, we have selected simultaneous GSPC and ME observations. This constraint reduces the number of data sets to 3 taken on 1984 July 9 (84/191 $- 191^{th}$ day of 1984), 1984 November 2$-$3 (85/307$-$308), and 1985 September 14 (85/257). These data files are referred to here as set-1, set-2 and set-3 respectively, and the number of PH channels, corresponding file names in Done et al. are given in Table 1.

We performed a careful check on the energy scale and mutual area calibration of the two detectors (Ar and GSPC), following the method given in Rajeev et al. (1994). The Ar detector is the most used and well understood of all the three non-imaging detectors in the EXOSAT Observatory and we have suitably adjusted the energy gain of the GSPC detector with respect to the Ar detector. The area corrections were made on the Ar data and these corrections can be larger than those found for Cyg X-3 by Rajeev et al. due to differences in the durations of observations. The relative gain and area corrections are also given in Table 1. For set-3 the GSPC gain has to be corrected by 3.2%. It was found by Rajeev et al. (1994) that the GSPC gain can vary even within an observation and since such large corrections are unreliable we have not used the data from set-3 for further analysis. The set-2 data has better GSPC gain setting (gain 2) and it has Ar data in finer bins. Further, the hard X-ray flux density at 100 keV was about 8.4×10^{-4} photons cm^{-2} s^{-1} keV^{-1} in 1984 October (McConnell et al. 1989; Ubertini et al. 1991). This value is within 25% of the flux measured by us in 1992 April. Hence we can conclude that the set-2 data pertains to the γ_2 state of the source and we have used this data for further analysis.

We have attempted a combined fit to the EXOSAT ME Ar data ($2 - 20$ keV), GSPC data ($5 - 16$ keV) and XMPC data ($20 - 100$ keV). The ultra-soft component modeled as Gaussian lines in Barr and van der Woerd (1990) does not contribute significantly above 2 keV. We have modeled the low energy component as a blackbody emission. The interstellar neutral absorption in the line of sight to Cyg X-1 is kept fixed at 7×10^{21} cm^{-2} and the absorption cross section given by Morrison and McCommon (1983) has been used. We have restricted the iron line energy between 6.3 and 6.5 keV and line width between 0.1 and 0.2 keV, consistent with the ASCA measurements (Ebisawa et al. 1996). For the continuum we have considered the model involving the reflection of power-law photons from an ionized disk (pliref) developed by Done et al. (1992). Since it is known that at higher energies Sunyaev-Titarchuk Comptonisation model (CompST) explains the spectral steepening, we have also considered the CompST model along with a variant of CompST : partial covering (pcfabs) of CompST. Using a model consisting of a low energy absorption (abs), blackbody emission (bbody) and Gaussian line at soft X-ray energies and pliref, CompST or partial covering of CompST at higher energies, we have attempted a combined fit to EXOSAT Ar, GSPC and XMPC data. For the reflection model the disk temperature is kept fixed at 10^5 K and the disk inclination is kept fixed at 30° (Done et al. 1992).

The normalization constant for the XMPC data is kept as a free parameter. Best fit parameters of the models along with nominal one sigma errors are given in Table 2. The relative normalization constant for XMPC data is determined to be 0.64. As can be seen from the table, the CompST model alone is inadequate to describe the continuum (reduced χ^2_{min} of 1.5). The reflection model as well as the partial covering of the CompST give statistically acceptable fits to the data (reduced χ^2_{min} close to 1), though the latter requires an extremely high value of N_H ($> 10^{24}$ cm^{-2}) covering 18% of the flux. Essentially, both the models imply that over and above a power law continuum there exists an extra emission above about 10 keV.

Done et al. (1992) fitted data from EXOSAT ME Ar, GSPC and HEAO-1 A2 over $5 - 50$ keV with a model consisting of low energy absorption, iron K_α line modeled with Gaussian and reflection of power-law photons from ionized accretion disk (pliref). They have fitted data from various detectors separately, whereas we have carried out simultaneous spectral fit to EXOSAT ME Ar, GSPC and XMPC data spanning much broader energy range of $2 - 100$ keV. Model parameters obtained here are consistent with those obtained by Done et al.

In Fig. 5 the observed count rate spectrum for Ar, GSPC and XMPC (layer 1 and layer 2+3) are shown. The best fit reflection model, convolved with the individual responses is shown as histogram. The residuals to the data are shown in the lower panel of the figure, as contribution to χ^2. The deconvolved spectra are shown in Fig. 6. The blackbody component, the Gaussian line and the reflection component are shown separately as his-

Table 1. Details of the EXOSAT observations of Cyg X-1

	Observation date		File name[1]	Duration (s)	PH channels	Area correction	Gain	Gain correction
set-1	1984 Jul 9	Ar	02me	1357	32	-2.0%	-	-
	(84/191)	GSPC	08	19790	256	-	1	0.0%
set-2	1984 Nov 2	Ar	17me	4500	64	-4.0%	-	-
	(84/307)	GSPC	13	5568	256	-	2	0.0%
set-3	1985 Sep 14	Ar	15me	10897.5	64	7.0%	-	-
	(85/257)	GSPC	09	27969	256	-	1	-3.2%

[1]File name, as given in Done et al. (1992)

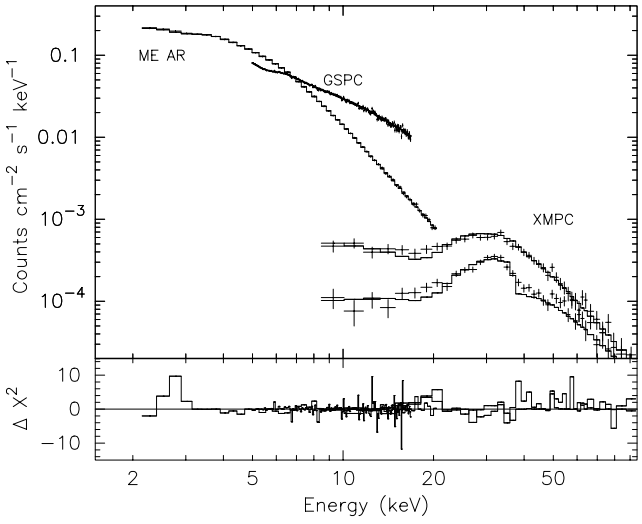

Fig. 5. The observed count rate spectra from Cyg X-1 obtained from EXOSAT ME Ar and GSPC are shown along with the XMPC data. The best fit ionized reflection model (along with low energy absorption, low energy blackbody, and a Gaussian line), obtained from a simultaneous fit to the three detectors, is shown as histograms, after convolving through individual detector response functions. The residuals are shown in the lower panel of the figure as contribution to the χ^2.

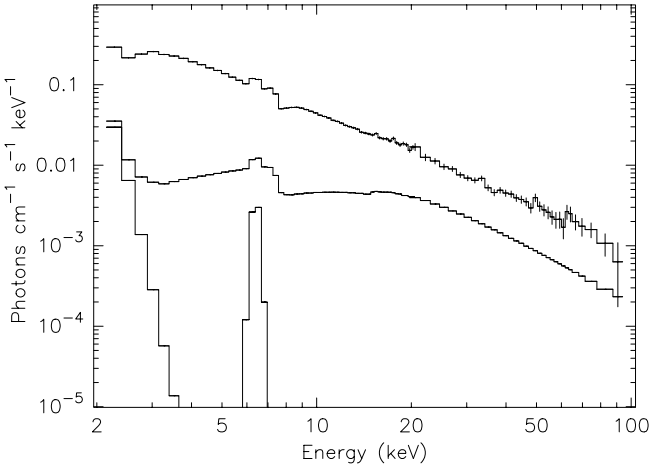

Fig. 6. Deconvolved spectrum of Cyg X-1 obtained from Ar, GSPC and XMPC detectors. For clarity, at a given energy, data from only one detector is shown. The contribution from individual model components (blackbody, Gaussian line and the reflection component) are shown as histograms.

tograms. For clarity, the unfolded data points are shown in a non-overlapping manner.

3.2. The OSSE data and simultaneous spectral fit to XMPC and OSSE data

The spectrum of Cyg X-1 below 100 keV is essentially a power-law (see Fig.6). The spectral turnover occurs above about 200 keV and it is essential to include high energy data for a proper modeling of the continuum. For this purpose we have analysed the archival data obtained from the Oriented Scintillation Spectrometer Experiment (OSSE) on-board Compton Gamma Ray Observatory (CGRO). The OSSE consists of four identical NaI-CsI phoswich detectors sensitive to gamma rays with energy 50 keV $-$ 10 MeV. Each detector has an effective area of $\sim$ 500 cm^2 at 511 keV (Johnson et al. 1993). Cyg X-1 was observed by OSSE on 17 occasions from 1991 to 1995. We have extracted the longest data stretch, with 100 keV flux density within 10% of XMPC from OSSE archives. These observations were carried out from 1991 May 30 to 1991 June 7 (1991/150$-$158), in viewing period 2. Total duration of observations is 24.5 $\times$ 10^4 seconds and the observed flux density at 100 keV is 6.04 $\times$ 10^{-4} cm^{-2} s^{-1} keV^{-1}. The 45 $-$ 140 keV flux obtained from an analysis of the OSSE data shows that the source remained in between the historic γ_1 and γ_2 state, except for a deep super-low state in the beginning of 1994 (see Fig 1. of Phlips et al. 1996).

Since this conclusion is in contradiction with the conclusion obtained by Ling et al. that the source generally remains in γ_2 state, we have obtained the archival BATSE earth occultation data. It is found that between 1991 and 1993, the source had an average $45 - 140$ keV flux of 0.11, varying between 0.07 and 0.18 with a standard deviation of 0.02, without showing any indication of a trend in the light curve (fluxes are in units of photons cm^{-2} s^{-1}). Since this behavior is similar to the γ_2 behavior, we conclude that the source was in the γ_2 state during 1991-1993. The differences in the absolute values of the fluxes could be due to the different overall calibration of the instruments (the average BATSE flux is 25% lower than the average γ_2 flux obtained by HEAO-3).

We have carried out a simultaneous spectral fit to the XMPC and OSSE data, with the relative normalization as a free parameter, with various spectral models. We have selected OSSE data from 50 to 500 keV. We have tried to fit this data over energy range $20 - 500$ keV with Sunyaev-Titarchuk Comptonisation (CompST) model and power law with exponential cutoff. The best fit model parameters along with the nominal one sigma errors are given in Table 3. It can be seen from the table that a single CompST is totally inadequate to explain the 20 to 500 keV spectrum of Cyg X-1 (reduced $\chi^2_{min} > 10$). The cutoff power law model too is statistically unacceptable to fit the data (reduced $\chi^2_{min} >$ about 2). On the other hand, the continuum over $20 - 500$ keV band is best explained by two CompSTs, with temperatures (kT$_e$) 77.5 and 28.4 keV and optical depths (τ) 2.0 and 11.1, respectively. Relative normalization of the OSSE detector with respect to XMPC is determined to be 0.85. In Table 3, as well as in the subsequent tables, errors in the parameter values are not given whenever reduced χ^2_{min} is greater than 2.

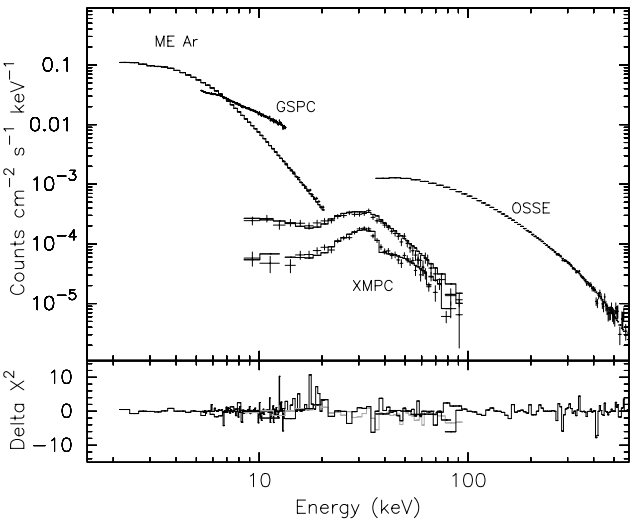

Fig. 7. The observed count rate spectra from Cyg X-1 obtained from EXOSAT ME Ar, EXOSAT GSPC, XMPC and OSSE are shown. The best fit model consisting of low energy absorption, low energy blackbody, Gaussian line, absorption edge and two CompSTs convolved through individual detector responses is shown as histogram. The residuals to the model fit are shown in the lower panel of the figure as contribution to the χ^2.

3.3. Wide band ($2 - 500$ keV) spectrum

We have attempted a wide band spectral fit over $2 - 500$ keV, combining EXOSAT Ar, GSPC, XMPC and OSSE data, using the above mentioned spectral models. The low energy components are modeled as Galactic absorption, blackbody and Gaussian line. A single CompST for the high energy continuum is inadequate to fit the data (reduced $\chi^2_{min} \sim 6.5$). Reflection of a power-law is also inadequate since there is a spectral turnover above 200 keV. We have also attempted to fit a model consisting of reflection of a CompST spectrum, which, we find, over-predicts the spectrum above 200 keV. A model consisting of two CompSTs, however, gives a reasonable value for the reduced χ^2_{min} (1.23). It is known that Cyg X-1 low energy spectrum has an edge like feature near 7.5 keV (Ebisawa et al. 1996), which was taken into account by the reflection spectrum in our combined fitting of the EXOSAT and XMPC data (see Fig. 6). To explicitly account for this discontinuity, we also included an edge feature in the model. The low energy component (which is modeled as a blackbody) generally shows a tendency to be correlated with the low energy absorption. To account for this, we also let the absorption vary. These modifications in the model improved the χ^2_{min} by 64 (reduced χ^2_{min} 1.09). The best fit spectral model consists of the soft excess modeled as a blackbody emission with temperature (kT$_{bb}$) 0.33 ± 0.04 keV, iron line modeled as a Gaussian with energy 6.47 ± 0.15 keV and width 0.1 keV, continuum consisting of two Sunyaev-Titarchuk inverse Compton models with electron temperatures kT$_e$ 80.2 ± 1.7 and 29.7 ± 0.6, with optical depths 1.96 ± 0.04 and 8.3 ± 0.8, respectively, along with line of sight absorption of $(2.34\pm0.31) \times 10^{22}$ cm^{-2}. The derived edge energy is 7.76 ± 0.12 keV and the equivalent width of the iron line is 17.2 eV. The best fit spectral parameters for this model and also for a model where continuum is modeled by single CompST are given in Table 4. The normalisation constant for the blackbody radiation is the radius of the emitting region and for the best-fit model it is 75 km for a distance of 2.5 kpc and the blackbody luminosity is 8×10^{36} ergs s^{-1} (or 13×10^{37} ergs s^{-1} for a distance of 10 kpc). Comparison of these parameters with those obtained for combined fit to XMPC and OSSE data (Table 3) shows that the parameters are consistent in both cases and are better constrained in $2 - 500$ keV spectral fit, because of the larger dynamic range. The observed count rate spectrum along with the best fit model spectrum convolved with individual detector response matrices are shown in Fig. 7. Residuals are shown in the lower panel of the figure as contribution to the χ^2. The deconvolved spectrum is shown in Fig. 8 along with the contribution from the individual model components. For the sake of clarity only EXOSAT Me Ar, XMPC top layer and OSSE data are shown here in a non-overlapping manner.

Table 2. Spectral parameters of Cyg X-1 in 2 − 100 keV band

Model component	Parameters[1]	value	value	value
abs	N_H (10^{22} cm^{-2})	0.7	0.7	0.7
bbody	kT_{bb} (keV)	0.14±0.03	0.14±0.03	0.14±0.03
	R (km)	1564±220	2056±290	2500±350
Gaussian	E_{Line} (keV)	6.40±0.15	6.42±0.07	6.52±0.06
	σ (keV)	0.1±0.9	0.2±0.3	0.2±0.2
	K_{Line}	1.73±0.99	4.00±0.71	6.44±0.93
pliref	α	1.84±0.01		
	$\Omega/2\pi$	0.73±0.07		
	ξ	56.0±26.6		
	norm	2.70±0.04		
CompST	kT_e (keV)		30.9±4.3	41.9±17.3
	τ		3.8±0.3	3.0±0.7
	norm		2.40±0.02	3.20±0.08
pcfabs	N_H (10^{22} cm^{-2})			262±25
	cov. fract.			0.180±0.014
χ^2_{min} (dof)		369.4 (341)	509.1 (342)	369 (340)

[1]The normalisation constants for the various components are : radius of emitting region of the blackbody for a distance of 2.5 kpc; in units of 10^{-3} photons cm^{-2} s^{-1} (total) for the Gaussian line; and photons cm^{-2} s^{-1} for CompST and pliref.

Table 3. Spectral parameters of Cyg X-1 in 20 − 500 keV band

Model component	Parameters[1]	value	value	value
CompST	kT_e (keV)	52.5	77.51±1.79	
	τ	2.9	2.01±0.04	
	norm	2.0	2.71±0.30	
CompST	kT_e (keV)		28.45±1.26	
	τ		11.1±5.5	
	norm		$(1.52 \pm 2.21) \times 10^{-2}$	
cutoffpl	α			0.95
	cutoff energy (keV)			123.1
	norm			0.21
χ^2_{min} (dof)		2095 (204)	209.4 (201)	458.4 (204)

[1]The normalisation constants for the various components are in units of photons cm^{-2} s^{-1}.

Table 4. Spectral parameters for wide band spectrum of Cyg X-1 ($2 - 500$ keV)

Model component	Parameters[1]	value	value	value
abs	N_H (10^{22} cm^{-2})	0.7	0.7	2.34±0.31
bbody	kT_{bb} (keV)	0.13	0.23±0.03	0.33±0.04
	R (km)	4330	120±13	75±8
Gaussian	E_{Line} (keV)	6.33	6.477±0.063	6.47±0.15
	σ (keV)	0.2	0.2	0.1±0.5
	K_{Line}	5.23	4.17±0.82	1.6±1.1
Edge	E (keV)			7.76±0.12
	τ_{max}			(6.1±0.9) × 10^{-2}
CompST	kT_e (keV)	53.6	79.55±1.59	80.2±1.7
	τ	2.8	2.00±0.03	1.96±0.04
	norm	2.2	2.50±0.02	2.72±0.06
CompST	kT_e (keV)		29.36±0.53	29.7±0.6
	τ		8.12±0.56	8.3±0.8
	norm		(4.4±1.0) × 10^{-2}	(3.9±1.2) × 10^{-2}
χ^2_{min} (dof)		2727 (422)	516 (419)	452 (416)

[1]The normalisation constants for the various components are : radius of emitting region of the blackbody for a distance of 2.5 kpc; in units of 10^{-3} photons cm^{-2} s^{-1} (total) for the Gaussian line; and photons cm^{-2} s^{-1} for CompST and pliref.

4. Discussion

Recently Gierlinski et al. (1997) have made a simultaneous spectral fit to the $3 - 500$ keV data (with a break between 30 and 50 keV) obtained from the Ginga and OSSE observations. The complete spectrum of Cyg X-1 presented here, however, is the first attempt to fit the spectrum in a very wide band ($2 - 500$ keV) without any break in the data. The methodology adopted here implicitly makes the assumption that the factor of 2 variability observed in the γ_2 state is due to changes in the normalisation constants of the spectral components rather than any change in the spectral parameters themselves. This assumption is vindicated from the fact that acceptable values of χ^2_{min} are obtained for the complete spectral fit. Further, the data used in the present work has been utilised to examine the transition disk model (Misra et al. 1997a) and the conclusions did not change when simultaneous data was used to examine the same model (Misra et al. 1997b). The relative normalisation for the different detectors are used as parameters to be fitted in the fitting procedure. The differences in normalisation (36% between EXOSAT and XMPC and 15% between OSSE and XMPC) are of the same order as the variations seen in the γ_2 state. Further, when a χ^2 contour plot for the normalisation of XMPC with respect to the OSSE data and other parameters like τ is made, it is found that the normalisation (85%) is constrained within $\pm 1\%$.

When the high energy continuum is adequately modeled, the parameters obtained for the low energy are consistent with those found while analyzing higher resolution data like ASCA and ROSAT. The equivalent width of the iron line obtained from the ASCA data ($13 - 40$ eV) compares well with the result presented here (17 eV). The blackbody luminosity derived here (13×10^{37} ergs s^{-1} for a distance of 10 kpc) is comparable to the value of 7.5×10^{37} ergs s^{-1} derived from the ROSAT data by Balucinska-Church et al. (1995). The interstellar absorption derived here is a factor of 4-5 higher compared to that obtained from the ROSAT data (which is the same as the Galactic absorption). As pointed out earlier, for the energy band under consideration (> 2 keV) interstellar absorption and blackbody temperature are related to each other and we can only conclude that there exists a soft excess the magnitude of which is comparable to that obtained from earlier studies.

The high energy continuum is adequately modeled with the final reduced χ^2_{min} of 1.09. Since there is a clear break in the spectral shape near $300-500$ keV, it is evident that power law or reflection of power law cannot adequately explain the continuum. Further, a single component CompST is also not adequate to fit the continuum mainly because of an excess emission near

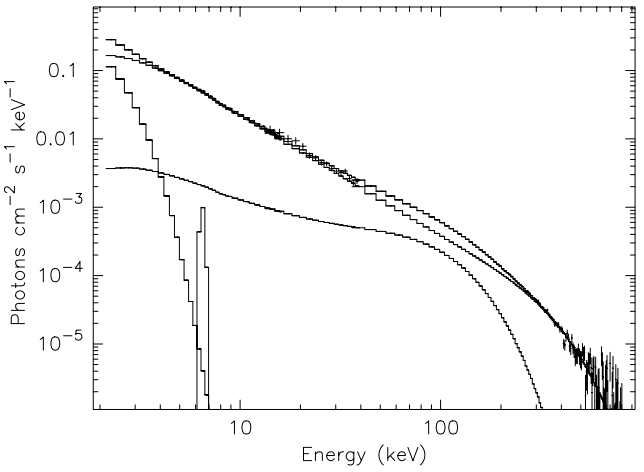

Fig. 8. The deconvolved spectra of Cyg X-1 obtained from EXOSAT ME Ar, XMPC and OSSE are shown. Contributions from individual model components (low energy blackbody of temperature 0.328 keV; Gaussian line at 6.47 keV and two CompSTs of temperatures 80.2 keV and 29.7 keV, respectively) are shown separately as histograms.

about 100 keV. We find that this excess cannot be modeled as a reflection of CompST model: to provide high reflection at 100 keV, it requires that the reflection component has to be dominant all the way up to 300 keV, which is not seen in the data (see Fig. 8).

Cutoff power-law produces satisfactory fit to the data above 50 keV (better than a single temperature CompST). It, however, cannot explain the continuum below 20 keV. Best fit cutoff-power-law in hard X-ray band underestimates the flux when extrapolated below 20 keV. Soft X-ray band requires steep power law (index ~ 1.7) and hence a cutoff power-law cannot explain the continuum completely. Phlips et al. (1996) have modeled OSSE data with an exponentially truncated power-law with reflection. This model, however, does not explain the continuum at lower energies, since power-law with photon index of 0.95 is not consistent with the low energy data.

There were a few attempts to model the wide band X-ray spectrum of Cyg X-1. Haardt et al. (1993) showed that a simulated spectrum of reflection of high temperature CompST (kT_e of 153 keV) agrees reasonably well with a low temperature CompST (kT_e of 63 keV) above 20 keV. What we find here is that when complete data is taken from 2 keV to 500 keV, single CompST leaves out a residual whose spectral shape is unlike a reflection component, but agrees reasonably well with another CompST component. Grebenev et al. (1993) on the other hand considered $3 - 1300$ keV data from the ART-P and SIGMA onboard the GRANAT satellite. They found that single CompST does not give an acceptable fit to the data. They, however, could reproduce the overall shape of the spectrum using a Monte-Carlo simulated Comptonisation spectra from an accretion disk, though the value of χ^2_{min} is not mentioned.

The results obtained by Gierlinski et al. (1997) using the simultaneous Ginga and OSSE data agrees with the broad conclusions obtained here viz., the wide band spectra demands an extra component near 100 keV. This component can be fit with several different analytical models. What the present work specifically showed is that the reasonable energy resolution in the medium energy band ($20 - 100$ keV) is important to constrain this component and the good energy resolution at low energies is also important to analytically formulate this component since the extra spectral component has sufficient flux below 10 keV. A simultaneous observation with ASCA and XTE and a rigorous spectral modeling will help in clarifying the spectral shape of Cyg X-1.

As pointed out by Grebenev et al. (1993), it may be a little naive to expect a single temperature plasma in an accretion disk. Further, at energies near 511 keV one has to include the relativistic Klein-Nishima cross-section of Compton scattering, which may change the spectral shape at these energies. The spectral shape obtained here, however, gives an extremely satisfactory fit to the data all the way from 2 keV to 500 keV. In the following we explore the various spectral models obtained here in light of the accretion disk theory around black holes developed by Chakrabarti and Titarchuk (1995).

Chakrabarti and Titarchuk (1995) have taken a complete solution of viscous transonic equations and demonstrated that the accretion disk has a highly viscous Keplerian part which resides on the equatorial plane and a sub-Keplerian component which resides above and below it. The sub-Keplerian component can form a standing shock wave (or, more generally, a centrifugal barrier supported dense region) which heats up the disk to a high temperature. The X-ray spectrum emitted from disks has various components: the Shakura-Sunyaev disk emission is at low energies and it may be identified with the low energy blackbody component. The bulk of the emission comes from cooling emission from Comptonisation which may be approximated to the CompST model derived here with a temperature of 80 keV. The second CompST model may be an approximation for the hard radiation reflected from the Shakura-Sunyaev disk along the observer. Another similarity between the the fitted model and the Chakrabarti-Titarchuk model is the very low equivalent width for the iron line. Hence it appears that the various spectral components obtained in the present study can be identified with the spectral models derived by Chakrabarti and Titarchuk (1995). It will be interesting to directly fit the Chakrabarti and Titarchuk (1995) model to the data.

5. Conclusions

We have analysed a wide band X-ray spectrum of Cyg X-1 and have obtained a statistically acceptable fit to the $2 - 500$ keV data. For this purpose, we have made hard X-ray observations using a balloon-borne large area xenon filled multi-anode proportional counter (XMPC) telescope. The response matrix of the detectors were calculated using a Monte-Carlo routine and the systematic errors in the data are brought down to a very low level. To extend the bandwidth, archival EXOSAT and OSSE data were obtained and a combined spectral fit to the data was attempted. The data in different energy bands, though not simultaneous, pertain to the γ_2 state of the source. We have assumed

that the variations in the source intensity in the γ_2 state is mainly due to the variations in the normalisations of the spectral components rather than any change in the spectral parameters. The main conclusions of this work are:

1. Statistically acceptable spectral fits were obtained using a model consisting of a i) interstellar absorption and low energy excess, ii) iron line and iron absorption edge, iii) continuum extending above 500 keV, and iv) an excess mainly near the energy region of 100 keV. The value of reduced χ^2_{min} is 1.09 for 416 degrees of freedom.

2. The low energy excess can be modeled as a blackbody with temperature 0.33 keV and luminosity of 8×10^{36} ergs s^{-1}. The interstellar equivalent neutral hydrogen column density is $2.3\pm0.3 \times 10^{22}$ cm^{-2}.

3. The derived values of line parameters are : the line energy 6.47$\pm$0.15 keV, the equivalent width of the line 17 eV and edge energy 7.76$\pm$0.12 keV.

4. The continuum can be explained by the Comptonisation model (Sunyaev and Titarchuk 1980) with an electron temperature of 80.2$\pm$1.7 keV and optical depth of 1.96$\pm$0.04.

5. The excess at higher energies can be explained as another CompST model with an electron temperature of 29.7$\pm$0.6 keV and optical depth of 8.3$\pm$0.8.

6. All these components have strong similarities with the spectral components predicted using the black-hole accretion model developed by Chakrabarti and Titarchuk (1985).

Acknowledgements. It is a pleasure to acknowledge the contribution of Shri M.R. Shah, Electronics Engineer-in-charge of this experiment, in the design, development and testing of the XMPC payload. We are also thankful to Shri D.K. Dedhia, Shri K. Mukherjee, Shri V.M. Gujar and Shri S.S. Mohite for their support in the fabrication of the payload. We thank the Balloon Support Instrumentation Group and the Balloon Flight Group for providing telemetry and telecommand packages and successfully conducting the balloon flight. Thanks are due to the EXOSAT database team for the archive and the CGRO team for the OSSE and the BATSE archives.

References

Arnaud, K. A., 1996, in: Jacoby G.H., Barnes J. (eds.) Astronomical Data Analysis Software and Systems V. ASP Conf. Series Vol. 101, San Francisco, p17.

Balucinska-Church, M. Belloni, T., Church, M.J. and Hasinger, G. 1995, A&A, 302, L5.

Balucinska-Church, M. and Barr, P. 1991, In *Iron Line Diagnostics in X-ray Sources*, Ed. A. Treves, G.C. Perola and L. Stella, Springer-Verlag, 130p.

Balucinska M. and Hasinger G. 1991, A&A, 241, 439.

Barr, P., White, N.E. and Page, C.G. 1985, MNRAS, 216, 65p.

Barr, P. and van der Woerd H. 1990, ApJL, 352, L41.

Chakrabarti, S.K., and Titarchuk, L.G., 1995, ApJ, 455, 623.

Döbereiner, S., Englhauser, J., Pietsch, W., Reppin, C., Trumper, J., Kendziorra, E., Kretschmar, P., Kunz, M., Maisack, M., Staubert, R., Efremov, V. and Sunyaev, R. 1995, A&A, 302, 115.

Done, C., Mulchaey, J.S., Mushotzky, R.F. and Arnaud, K.A. 1992, ApJ, 395, 275.

Ebisawa, K. 1991, PhD Thesis, University of Tokyo, Japan.

Ebisawa, K., Ueda, Y., Inoue, H., Tanaka, Y. and White, N.E. 1996, ApJ, 467, 419.

Gierlinski, M., Zdziarski, A. A., Done, C., Johnson, W. N., Ebisawa, K., Ueda, Y., Haardt, F., Phlips, B. 1997, MNRAS, 288, 958.

Grebenev, S., Sunyaev, R.A., Pavlinsky, M., Churazov, E., Gilfanov, M., Dyachkov, A., Khavenson, N., Sukhanov, K., Laurent, P., Ballet, J., Claret, A., Cordier, B., Jourdain, E., Niel, M., Pelaez, F. and Schmitz-Fraysse, M.C. 1993, A&ASS, 97, 281.

Haardt F., Done, C., Matt, G. and Fabian, A.C. 1993, ApJL, 411, L95.

Johnson, W.N., Kinzer, R.L., Kurfess, J.D., Strickman, M.S., Purcell, W.R., Grabelsky, D.A., Ulmer, M.P., Hillis, D.A., Jung, G.V., Cameron, R.A. 1993, ApJS, 86, 693.

Kitamoto, S., Miyamoto, S., Tanaka, Y., Ohashi, T., Kondo, Y., Tawara, Y. and Nakagawa, M. 1984, PASJ, 36, 731.

Kitamoto, S., Takahashi, K., Yamahita, K., Tanaka, Y. and Nagase, F. 1990, PASJ, 42, 85.

Laurent, P., Claret, A., Lebrun, F., Paul, J., Dennis, M., Barret, D., Bouchet, L., Mandrou, P., Sunyaev, R.A., Curazov, E., Gilfanov, M., Khavenson, N., Dyachkov, A., Novikov, B., Kremnev, R. and Kovtunenko, V. 1993, Adv. Space Res., 13, (12), 139.

Liang, E.P. and Nolan P.L. 1984, Space Sci. Rev., 38, 353.

Ling , J.C., Mahoney, W.A., Wheaton, W.A. and Jacobson, A.S. 1983, ApJ, 275, 307.

Ling , J.C., Mahoney, W.A., Wheaton, W.A. and Jacobson, A.S. 1987, ApJL, 321, L117.

Marshall, F.E., Mushotzky, R.F., Petre, R. and Serlemitsos, P.S. 1993, ApJ, 419, 301.

McConnell, M.L., Forrest, D.J., Owens, A., Dumphy, P.P., Vestrand, W.T., Chupp, E.L. 1989, ApJ, 343, 317.

McConnell, M., Forrest, D., Ryan, J., Collmar, W., Schonfelder, V., Steinle, H., Strong, A., van Dijk, R., Hermsen, W., and Bennett, K., 1994, ApJ, 424, 933.

Misra, R., Chitnis, V.R., Melia, F., Rao, A.R. 1997a, ApJ, 487,388.

Misra, R., Chitnis, V.R., Melia, F. 1997b, ApJ, in press.

Morrison, R. and McCammon, D. 1983, ApJ, 270, 119.

Nolan, P.L., Gruber, D.E., Knight, F.R., Matteson, J.L., Rothschild, R.E., Marshall, F.E., Levine, A.M. and Primini, F.A. 1981, Nat, 293, 275.

Peacock, A., Andresen, R.D., Manzo, G., Taylor, B.G., Villa, G., Re, S., Ives, J.C., Kellock, S. 1981, Space Sci. Rev., 30, 525.

Phlips B.F., Jung, G.V., Leising, M.D., Grove, J.E., Johnson, W.N., Kinzer, R.L., Kroeger, R.A., Kurfess, J.D., Strickman, M.S., Grabelsky, D.A., Matz, S.M., Purcell, W.R., Ulmer, M.P., and McNaron-Brown, K. 1996, ApJ, 465, 907.

Rajeev, M.R., Chitnis, V.R., Rao, A.R. and Singh, K.P. 1994, ApJ, 424, 376.

Rao, A.R., Agrawal, P.C., Manchanda, R.K. and Shah, M.R. 1987, Adv. Space Res. 7, (7), 129.

Rao, A.R., Agrawal, P.C. and Manchanda, R.K. 1991, A&A, 241, 127.

Salotti, L., Ballet, J., Cordier, B. et al. 1992, A&A, 253, 145.

Sunyaev, R.A. and Trumper, J. 1979, Nat, 279, 506.

Sunyaev, R.A. and Titarchuk L.G. 1980, A&A, 86, 121.

Tanaka, Y. 1991, In *Iron Line Diagnostics in X-ray Sources*, Ed. A. Treves, G.C. Perola and L. Stella, Springer-Verlag, 98p.

Turner, M.J.L., Smith, A. and Zimmermann, H.U. 1981, Space Sci. Rev., 30, 513.

Ubertini, P., Bazzano, A., Perotti, F., Quadrini, E., Court, A., Dean, A.J., Dipper, N., Lewis, R., Bassani, L. and Stephen, J.B. 1991, ApJ, 366, 544.

This article was processed by the author using Springer-Verlag LaTeX A&A style file *L-AA* version 3.